

## Imaging and Localized Spectroscopy of $^{13}\text{C}$ by Polarization Transfer

HONG N. YEUNG AND SCOTT D. SWANSON

*Department of Radiology, University of Michigan Medical Center, Ann Arbor, Michigan 48109*

Received November 3, 1988; revised January 23, 1989

The biological applications of  $^{13}\text{C}$  magnetic resonance spectroscopy are well known (1-5). Recently, there was evidence (6-9) suggesting that the citrate peak in the  $^{13}\text{C}$  spectrum may be useful as a marker for human prostate cancer. It was found in human prostate that the citrate concentration is small in the normal gland, negligible in malignant tumors (8), and increased markedly in tissues with benign prostatic hypertrophy (BPH) (8, 9). While this evidence suggests citrate as possibly a specific marker for malignant prostatic tumor and BPH, it also underscores the problem in applying NMR spectroscopic techniques without localization under *in vivo* conditions where prostatic malignancy is often, if not always, accompanied by BPH.

There are two possible solutions to the above problem. One is through multidimensional chemical-shift imaging (10, 11) and the other, localized spectroscopy. For carbon, either one of these two approaches presents many challenging problems. First, one must deal with the problem of low sensitivity and long  $T_1$ . Second, because carbon has a low  $\gamma$ , one needs four times as much gradient strength in imaging or localization of carbon as that of hydrogen. Third, since carbon has large chemical shifts, it is often difficult to separate the spatial from the spectral information. By using polarization transfer techniques, such as INEPT (12, 13) or DEPT (14, 15), the problems associated with low  $\gamma$  nuclei, such as carbon, are converted into those of protons which are much easier to solve. Recently this idea was exploited by Norris *et al.* (16), who applied a one-dimensional ISIS sequence (17) on the protons for the localization of carbon.

In this Communication, we will demonstrate an alternative technique of carbon selection based on the idea mentioned above and the conventional plane excitation method commonly used in proton imaging. In this scheme, plane selection of carbon is obtained by selective proton enhancement. We will also demonstrate that one can gain a similar type of enhancement in carbon imaging by applying phase encoding on the proton, instead of the carbon, polarization. We shall call this an indirect spin-warp method.

Figure 1 shows the method of localization of carbon by selective enhancement through excitation of hydrogen. The RF section of the pulse sequence in Fig. 1 is a DEPT sequence with a shaped proton  $\pi/2$  pulse. Since the phase-cycling scheme of the DEPT sequence is so designed that only the proton-enhanced nuclei are observed

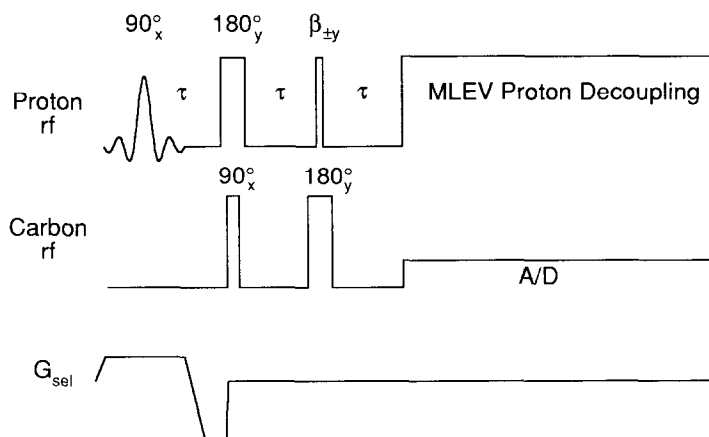


FIG. 1. Pulse sequence for plane selection of carbon nuclei through selective excitation of protons by DEPT ( $\tau = 1/2J$ ).

(all others are canceled), the profile of the carbon selection plane should be as good as one can achieve with the proton plane. Although DEPT is chosen here for the illustration of this localization technique, similar results can be expected if an INEPT sequence is used.

Figure 2 shows a hybrid three-dimensional (1D spectral and 2D spatial) imaging/spectroscopy sequence using an INEPT-like (Fig. 2A) and a DEPT (Fig. 2B) technique. Note here that in either of these hybrid imaging/spectroscopy schemes, one has two ways of applying a phase-encoding gradient(s) for spatial information. One is to apply it directly on the carbon transverse polarization (shown as solid lines in Figs. 2A and 2B) immediately after the  $\pi/2$  carbon pulse. The other is to apply the phase encoding indirectly upon the proton spins (shown as broken lines in Figs. 2A and 2B) after the first  $\pi/2$  proton pulse. This indirect method of phase encoding can be considered another form of proton enhancement which in this instance is in spatial resolution. To implement this novel technique in spatial encoding, the encoded phase information must be acquired and combined in phase quadrature. This can be easily accomplished for INEPT by phase cycling the second  $\pi/2$  ( $\beta$  for DEPT) pulse on proton with a four-phase cycle ( $0, \pi/2, \pi, 3\pi/2$  with respect to the first  $\pi/2$  proton pulse) and by routing the corresponding data lines in their proper phase order. The reason is that components of the spin-coupled proton transverse polarization, which bear spatial information after the encoding pulse, are transformed into a biphasic vector along the  $z$  axis, upon the action of the second  $\pi/2$  (or  $\beta$  for DEPT) proton pulse. Thus, if the  $\pi/2$  proton pulse is only phase-alternated, as normally required in both DEPT and INEPT, one component of the information will be lost which results in an ambiguity of the sign of the position coordinate ( $y$ , for example) one intends to encode. This ambiguity arises from the fact that the two pieces of binary information ( $+y$  or  $-y$  and  $J+$  or  $J-$ ) are piled upon a single bipolar axis. The consequence is that two of the four possible states are aliases of each other. The reconstructed

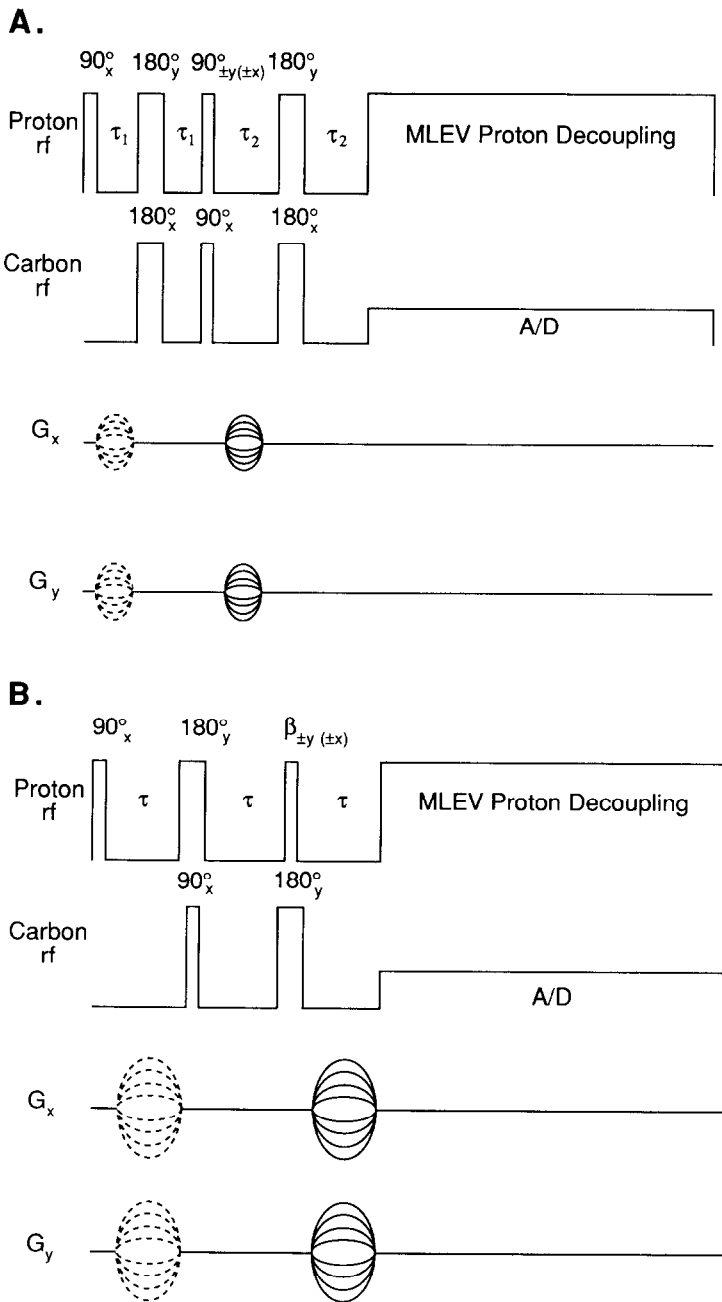


FIG. 2. Pulse sequences for  $^{13}\text{C}$  chemical-shift imaging by polarization transfer. (A) Refocused INEPT ( $\tau_1 = 1/4J$  and  $\tau_2 = 1.5\tau_1$ ) and (B) DEPT ( $\tau = 1/2J$ ).

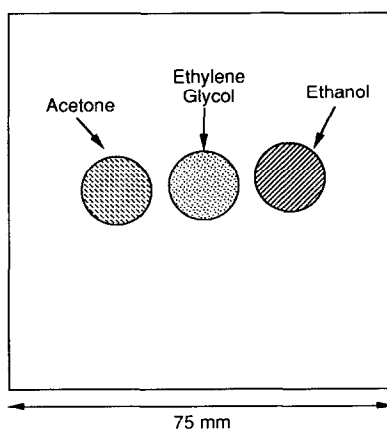


FIG. 3. Phantom used for the demonstration of proton-enhanced,  $^{13}\text{C}$ -localized spectroscopy and chemical-shift imaging. The three vials contained, from right to left, naturally abundant ethanol, ethylene glycol, and acetone. Each vial was 15 mm in diameter and 35 mm long.

images therefore will show an object along with its mirror image in  $y$ . By repeating the experiment with the second  $\pi/2$  (or  $\beta$ ) pulse on the proton in phase quadrature with respect to the first, this ambiguity is removed. The resulting data lines so combined will yield a reconstructed image free of ambiguity which contains no mirror image of the object (see Fig. 5).

Experiments were performed with the aid of a GE 2.0 T CSI system (31 cm bore diameter) equipped with a second RF channel for double resonance. The probe consisted of two homebuilt, Helmholtz RF coils positioned so that the  $B_1$  fields are orthogonal to each other and tuned, respectively, at the proton and carbon resonance frequencies. The diameter of the outside proton coil is 7 cm and that of the inside carbon coil, only slightly smaller. The RF power was adjusted on each channel so that the proton and carbon  $\pi/2$  pulse widths were 120  $\mu\text{s}$ . The proton decoupling scheme employed is a phase-alternated broadband MLEV sequence (18) provided by the manufacturer. Magnet shimming was performed using the proton signal from the sample studied before each experiment. The phantom consisted of three sample tubes arranged in a linear array (Fig. 3). They contained, respectively, naturally abundant ethanol, ethylene glycol, and acetone.

Localization of carbon using indirect selective excitation on protons is demonstrated in Fig. 4. By selective irradiation of the protons of the tubes at different locations, a routine proton imaging technique, the carbon signal of different sample tubes can be selected at will by polarization transfer (in this instance, using the DEPT sequence).

Figure 5 shows the contour plots of the carbon image of the same phantom (Fig. 3) by projecting the hybrid three-dimensional data set along the chemical-shift axis and along the third spatial dimension (i.e., the image intensity at each pixel represents the total sum of all spectral components projected on the imaged plane at that particular coordinate). Figure 5A shows the image with the conventional direct phase en-

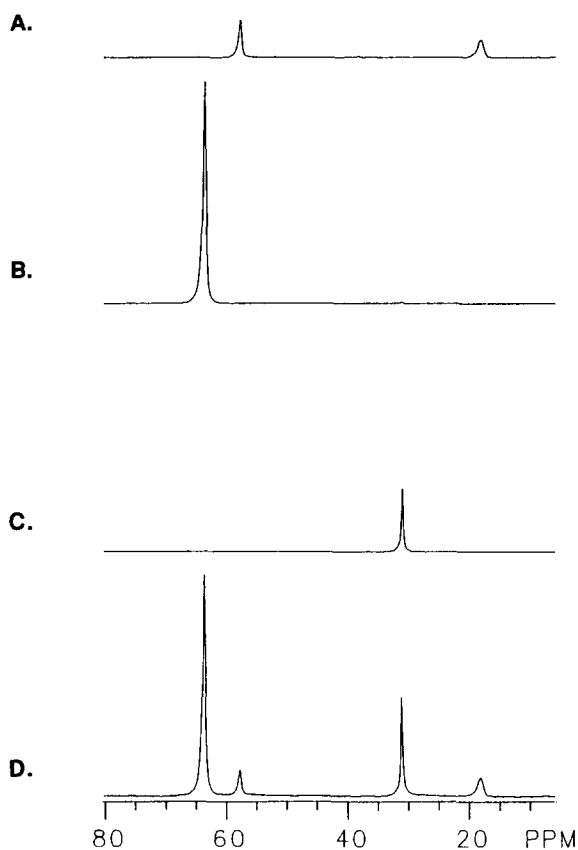


FIG. 4. Localized  $^{13}\text{C}$  spectra from the phantom pictured in Fig. 3 using the plane selection DEPT pulse sequence (Fig. 1). (A)  $^{13}\text{C}$  spectrum of a plane (15 mm thick) which is offset  $-20$  mm from the center of the phantom, selecting the ethanol vial. (B)  $^{13}\text{C}$  spectrum of a 15 mm plane with no offset, selecting the ethylene glycol vial. (C)  $^{13}\text{C}$  spectrum of a 15 mm plane which is offset  $+20$  mm from the center, selecting the acetone vial. (D)  $^{13}\text{C}$  spectrum of the phantom with no plane selection. The spectra with plane selection (A–C) employed a 2 ms, single-lobe sinc pulse and a gradient strength of 0.78 mT/m. All spectra were acquired using a 3 kHz sweep width, 100 averages, and a 1 s repetition rate.

coding on the carbon polarization. Figure 5B shows the corresponding image using the same technique except that the phase encodings were performed indirectly through the proton polarization (and with the quadrature phase cycling as described earlier). By comparing these two images, the resolution enhancement of the indirect method is vividly demonstrated.

While the method of indirect localization proposed above is only one-dimensional, one may speculate that it can be, at least in principle, extended to two or three dimensions. One possible approach is to use consecutive selective pulses on the  $\pi/2$ ,  $\pi$ , and  $\beta$  proton pulses in a manner similar in spirit to the SPARS scheme (19) applied in localization of the protons.

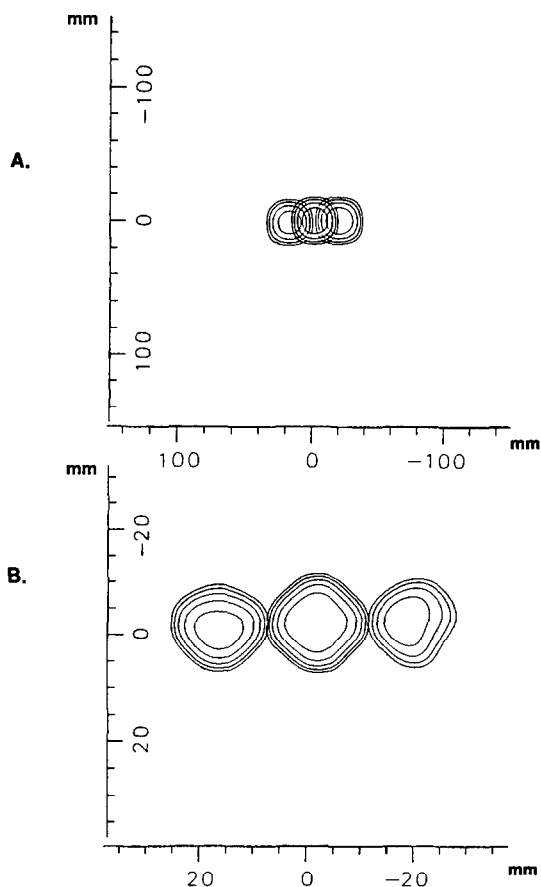


FIG. 5. Phantom results of carbon imaging using the DEPT chemical-shift imaging pulse sequence (Fig. 2B). (A) Direct phase encoding via carbon polarization and (B) indirect spin warp via proton polarization with the same gradient strengths as in (A). Each image is a projection along the  $z$  axis and the chemical-shift axis and is the sum of three independently reconstructed images of ethanol, ethylene glycol, and acetone. The time-domain data consisted of  $1024$  complex points with  $16$  phase-encoding steps in both the  $x$  and the  $y$  directions, yielding a  $1024 \times 16 \times 16$  array. The  $16 \times 16$   $k$ -space array was zero-filled to an array of  $128 \times 128$  points and Fourier transformed in both dimensions to yield the images presented in the figure. The images were obtained with four averages per data line, a sweep width of  $3.5$  kHz, and a repetition rate of  $1$  s. The total acquisition time was  $23.8$  min for (A) and  $47.6$  min for (B).

#### REFERENCES

1. R. G. SHULMAN, T. R. BROWN, K. UGURBIL, S. OGAWA, S. M., COHEN, AND J. A. DEN HOLLANDER, *Science* **205**, 160 (1979).
2. K. WÜTHRICH, "NMR in Biological Research: Peptides and Proteins," Elsevier, New York, 1976.
3. J. R. ALGER, L. O. SILLERUD, K. L. BEHAR, R. J. GILLIES, R. G. SHULMAN, R. E. GORDON, D. SHAW, AND P. E. HANLEY, *Science* **214**, 660 (1981).
4. L. O. SILLERUD AND R. G. SHULMAN, *Biochemistry* **22**, 1087 (1983).
5. C. H. HAN AND L. O. SILLERUD, *Magn. Reson. Med.* **3**, 626 (1986).

6. R. B. FRANKLIN, L. C. COSTELLO, AND G. K. LITTLETON, *Enzyme* **22**, 45 (1977).
7. J. F. COOPER AND I. FARID, *J. Urol.* **92**, 533 (1964).
8. K. R. HALLIDAY, C. FENOGLIO-PREISER, AND L. O. SILLERUD, *Magn. Reson. Med.* **7**, 384 (1988).
9. S. D. SWANSON, L. E. QUINT, AND H. N. YEUNG, *Magn. Reson. Med.*, submitted.
10. T. R. BROWN, B. M. KINCAID, AND K. UGURBIL, *Proc. Natl. Acad. Sci. USA* **79**, 3523 (1982).
11. A. A. MAUDSLEY, S. K. HILAL, W. H. PERMAN, AND H. E. SIMON, *J. Magn. Reson.* **51**, 147 (1983).
12. G. A. MORRIS AND R. FREEMAN, *J. Am. Chem. Soc.* **101**, 760 (1979).
13. D. P. BURUM AND R. R. ERNST, *J. Magn. Reson.* **39**, 163 (1980).
14. D. M. DODDRELL, D. T. PEGG, AND M. R. BENDAL, *J. Magn. Reson.* **48**, 323 (1982).
15. M. R. BENDALL AND D. T. PEGG, *J. Magn. Reson.* **53**, 272 (1983).
16. D. G. NORRIS, N. SCHUFF, AND D. LEIBFRITZ, *J. Magn. Reson.* **78**, 362 (1988).
17. R. J. ORDIDGE, A. CONNELLY, AND J. A. B. LOHMAN, *J. Magn. Reson.* **66**, 283 (1986).
18. M. H. LEVITT, R. FREEMAN, AND T. FRENKIEL, in "Advances in Magnetic Resonance (J. S. Waugh, Ed.), Vol. 11, p. 47, Academic Press, New York, 1983.
19. P. R. LUYTEN, C. M. ANDERSON, AND J. A. DEN HOLLANDER, *Magn. Reson. Med.* **4**, 431 (1987).